energies

MDPI

Article

Two-Stage Optimization Scheduling of Integrated Energy Systems Considering Demand Side Response

Shuang Zeng, Heng Zhang *, Fang Wang, Baoqun Zhang, Qiwen Ke and Chang Liu

State Grid Beijing Electric Power Company, Beijing 100075, China; zengshuang@bj.sgcc.com.cn (S.Z.); wangfang@bj.sgcc.com.cn (F.W.); zhangbaoqun@bj.sgcc.com.cn (B.Z.); keqiwen@bj.sgcc.com.cn (Q.K.); liuchangh@bj.sgcc.com.cn (C.L.)

* Correspondence: shaochen_336@163.com

Abstract: This study proposes a two-level optimization scheduling method for multi-region integrated energy systems (IESs) that considers dynamic time intervals within the day, addressing the diverse energy characteristics of electricity, heat, and cooling. The day-ahead scheduling aims to minimize daily operating costs by optimally regulating controllable elements. For intra-day scheduling, a predictive control-based dynamic rolling optimization model is utilized, with the upper-level model handling slower thermal energy fluctuations and the lower-level model managing faster electrical energy fluctuations. Building on the day-ahead plan, different time intervals are used for fast and slow layers. The slow layer establishes a decision index for command cycle intervals, dynamically adjusting based on ultra-short-term forecasts and incremental balance corrections. Case studies demonstrate that this method effectively leverages energy network characteristics, optimizes scheduling intervals, reduces adjustment costs, and enhances system performance, achieving coordinated operation of the IES network and multi-energy equipment.

Keywords: integrated energy system; two-level optimization scheduling method; generative adversarial network; dynamic time interval; intra-day scheduling

Citation: Zeng, S.; Zhang, H.; Wang, F.; Zhang, B.; Ke, Q.; Liu, C. Two-Stage Optimization Scheduling of Integrated Energy Systems Considering Demand Side Response. *Energies* **2024**, *17*, 5060. https://doi.org/10.3390/en17205060

Academic Editors: Michail Tsangas and Antonis A. Zorpas

Received: 5 August 2024
Revised: 24 August 2024
Accepted: 26 September 2024
Published: 11 October 2024

1. Introduction

With the rapid development of renewable energy and the improvement of energy utilization efficiency, sustainable energy development has become an urgent global demand [1,2]. The increasing share of solar, wind, and other renewable energies in power generation has driven the modernization and diversification of energy systems. Against this backdrop, the Integrated Energy System (IES) has emerged as an innovative energy solution, gradually becoming a focal point of research [3]. The IES integrates multiple energy subsystems, such as electricity, cooling, heating, and natural gas systems, to achieve synergies and complementarities among different energy forms, maximizing energy utilization efficiency and reducing carbon emissions [4,5].

He core concept of the IES is to leverage the complementary characteristics of various energy types and the principles of energy cascading utilization to optimize resource allocation, enhance overall system efficiency, and promote the transition towards low-carbon, efficient, and intelligent energy systems [6]. Literature [7] adopts a two-stage robust optimization method that addresses uncertainties in wind power and load, significantly improving the economic efficiency and reliability of electricity-gas-heat integrated multi-energy microgrids. Meanwhile, literature [8] explores the coordinated operation of hydrogen, electricity, and transportation systems, enhancing the overall system efficiency through the complementary effects of energy flows and providing practical guidance for the integration and optimization of multi-energy flows. Additionally, literature [9] proposes a distributed stochastic programming approach that reconfigures multi-energy distribution systems to enhance system resilience against external disturbances.

The IES comprises multiple subsystems, including electricity, cooling, and heating systems. The electricity supply system requires real-time energy balance with scheduling intervals at the second or minute level, classifying it as a fast dynamic system [10]. In contrast, due to the storage characteristics of gas pipelines and the thermal inertia of heat networks and building clusters, heating and gas supply subsystems typically have scheduling intervals in hours, making them slow dynamic systems [11,12]. The varying scheduling intervals and operational characteristics of these systems make IES scheduling optimization a complex multi-time-scale, multi-energy-flow optimization problem [13]. Solving the optimization of IES operations is crucial for improving the overall energy efficiency and renewable energy utilization, ultimately contributing to achieving carbon neutrality goals.

Multi-time-scale dual-layer optimization models primarily target day-ahead and intra-day scheduling plans. Current methods typically adopt static optimization [14,15] and dynamic optimization [16–18]. Model predictive control introduces closed-loop dynamic optimization with state feedback correction, which has increasingly been applied to intra-day scheduling in IESs. Literature [19] proposes a two-stage stochastic model, where the first stage uses a genetic algorithm to search for variables, and the second stage uses the Monte Carlo method to handle uncertainties and solve the optimization problem. Literature [20] proposes a dual-layer coordinated optimization method that integrates upper-layer equipment configuration with lower-layer energy storage parameters, further enhancing the stability and security of IES operations.

These studies generally perform large-time-scale rolling optimization for day-ahead scheduling plans, followed by minute-level adjustments based on real-time operational states during intra-day scheduling. However, these methods often use the same time scale across all energy layers, overlooking the time delay effects in different energy layers. Due to the varying dynamic characteristics of the electricity, gas, and thermal subsystems in IESs, using the same scheduling instruction interval may lead to over-scheduling of fast systems (e.g., electricity) while failing to accurately capture the dynamics of slow systems (e.g., heating and gas) [15,21]. Therefore, selecting appropriate scheduling intervals to balance the needs of both fast and slow systems is key to optimizing scheduling strategies. By incorporating real-time and predictive operational states, establishing a dual-layer scheduling model with dynamic time intervals will better address the challenges of multi-energy flow scheduling in IESs [22].

This paper addresses the intra-day scheduling problem of an IES by proposing a two-layer optimization scheduling strategy that considers dynamic time intervals. The main contributions of this paper are as follows:

(1) A multi-time scale IES intra-day dual-layer scheduling model is proposed. This model separates intra-day scheduling into an upper-layer thermal and cooling energy scheduling model and a lower-layer electrical energy scheduling model. By handling slower dynamics in the upper layer and faster dynamics in the lower layer, and dynamically updating ultra-short-term forecast information, the model improves the overall system efficiency.
(2) A method for dynamically adjusting scheduling instruction periods is established. This approach uses different time intervals for each layer (1 h for thermal and cooling, 15 min for electrical) to address time delay characteristics and ensure accurate and effective scheduling.
(3) The proposed model and method's effectiveness and superiority are validated through case studies. The results show improved coordination of device operations within the IES, enhancing system stability and economic performance.

The structure of this paper is as follows: Section 2 introduces the multi-region IES architecture considering electricity interconnection, Section 3 discusses the day-ahead economic scheduling model for the IES, Section 4 presents the day-ahead two-layer optimization strategy for the IES, Section 5 covers the case study analysis, and Section 6 concludes the paper.

2. Multi-Region IES Architecture Considering Electricity Interconnection

The multi-region IES architecture, as shown in Figure 1, includes three subsystems: cooling, heating, and electricity. The energy inputs mainly consist of grid electricity, distributed generations (DG), and natural gas system equipment, including gas turbines (GT), gas boilers (GB), and fuel cells (FC). The interconnection devices among the subsystems include electric boilers (EB), electric chillers (EC), and absorption chillers (AC), which enable the joint scheduling of the cooling, heating, and electricity systems. Each subsystem is equipped with energy storage devices: accumulators (for electricity), thermal storage tanks (for heat), and cold storage tanks (for cooling), to facilitate energy storage and release. The system load comprises uncontrollable base loads and controllable flexible loads. The flexible loads include shiftable loads, transferable loads, and reducible loads.

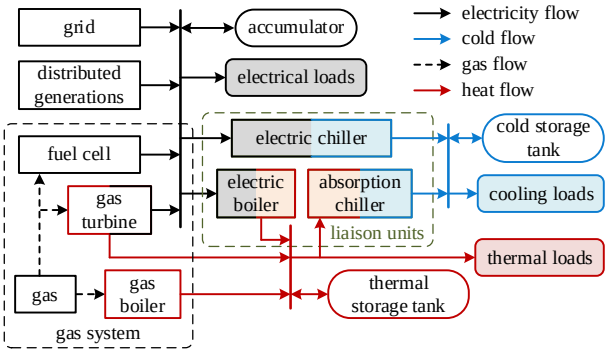

Figure 1. Integrated energy system architecture diagram.

3. Day-Ahead Economic Scheduling Model for IES

Day-ahead economic scheduling refers to the process of optimizing the economic operation of an IES based on forecasts of distributed generation output and load for the next 24 h, considering time-of-use electricity pricing from the grid side. The goal is to optimally regulate the output of controllable elements within the system to achieve the best economic performance for the IES. In practice, the scheduling process must be discretized; this paper divides the day-ahead scheduling process into 24 segments, with scheduling occurring every hour, and each segment is denoted as the *i*-th segment.

3.1. Day-Ahead Economic Scheduling Model Objective Function

The objective function for day-ahead optimization scheduling, with the goal of minimizing the daily operating cost of the IES is as follows:

$$\min F = F^{\text{grid}} + F^{\text{DG}} + F^{\text{gas}} + F^{\text{lia}} + F^{\text{sto}} + F^{\text{sh}} + F^{\text{tran}} + F^{\text{cut}} \tag{1}$$

3.1.1. System's Electricity Purchasing Cost F^{grid}

The system can purchase and sell electricity to the grid. The electricity purchasing cost, F^{grid}, is given by:

$$F^{\text{grid}} = \sum_{i=1}^{T} K_i^{\text{pur}} P_i^{\text{pur}} - \sum_{i=1}^{T} K_i^{\text{sell}} P_i^{\text{sell}} \tag{2}$$

where P_i^{pur} and P_i^{sell} represent the power purchased from and sold to the grid, respectively, and K_i^{pur} and K_i^{sell} are the corresponding purchase and sale prices.

3.1.2. Operating Cost of Distributed Generation Sources F^{DG}

The operating cost, F^{DG}, of distributed generation, including wind turbines and photovoltaic systems, is given by:

$$F^{\mathrm{DG}} = \sum_{i=1}^{T} K^{\mathrm{wind}} P_i^{\mathrm{wind}} + \sum_{i=1}^{T} K^{\mathrm{pv}} P_i^{\mathrm{pv}} \tag{3}$$

where P_i^{wind} and P_i^{pv} represent the power output from wind turbines and photovoltaic systems, respectively, and K^{wind} and K^{pv} are the operating cost coefficients for wind turbines and photovoltaic systems, respectively.

3.1.3. Natural Gas System Equipment Cost F^{gas}

The primary costs of natural gas system equipment include the cost of purchasing gas and the operational costs. Therefore, F^{gas} is given by:

$$\begin{cases} F^{\mathrm{GAS}} = \sum\limits_{i=1}^{T} K^{\mathrm{gas}} V_i^{\mathrm{GAS}} + \sum\limits_{i=1}^{T} K^{\mathrm{GAS}} P_i^{\mathrm{GAS}} \\ F^{\mathrm{gas}} = F^{\mathrm{GT}} + F^{\mathrm{GB}} + F^{\mathrm{FC}} \\ \mathrm{GAS} = [\mathrm{GT}, GB, \mathrm{FC}] \end{cases} \tag{4}$$

The cost of the natural gas system equipment mainly consists of natural gas purchasing costs and operating costs, where GAS represents the variables associated with the natural gas system equipment, F^{GAS} is the cost of the natural gas system equipment, P_i^{GAS} denotes the corresponding output, V_i^{GAS} is the corresponding gas purchase quantity, K^{gas} is the unit price of natural gas, and K^{GAS} is the corresponding operating cost coefficient. To accurately account for different types of outputs in the subsequent power and heat balance equations, the output of GT, P_i^{GT}, is divided into electrical power, $P_i^{\mathrm{GT.e}}$, and thermal power, $P_i^{\mathrm{GT.h}}$. This distinction helps the model ensure the balance and optimization of both power and heat demands in the system.

3.1.4. Operating Cost of Interconnection Devices for Each Subsystem F^{lia}

The operating cost of interconnection devices for each subsystem is related to their output. Assuming no additional costs are considered, F^{lia} is given by:

$$\begin{cases} F^{\mathrm{LIA}} = \sum\limits_{i=1}^{T} K^{\mathrm{LIA}} P_i^{\mathrm{LIA}} \\ F^{\mathrm{lia}} = F^{\mathrm{EB}} + F^{\mathrm{EC}} + F^{\mathrm{AC}} \\ \mathrm{LIA} = [\mathrm{EB}, \mathrm{EC}, \mathrm{AC}] \end{cases} \tag{5}$$

where LIA represents the variables associated with the interconnection devices for each subsystem, F^{LIA} is the operating cost of these interconnection devices, P_i^{LIA} denotes the corresponding output, and K^{LIA} is the corresponding operating cost coefficient.

3.1.5. Operating Cost of Energy Storage Devices F^{sto}

The energy storage devices incur aging costs due to charging and discharging, with depreciation expenses related to the power of charging and discharging. Assuming no other costs are considered, the cost, F^{sto}, of the energy storage devices is given by:

$$\begin{cases} F^{\mathrm{STO}} = \sum\limits_{i=1}^{T} K_{\mathrm{cha}}^{\mathrm{STO}} P_{\mathrm{cha}.i}^{\mathrm{STO}} X_{\mathrm{cha}.i}^{\mathrm{STO}} + \sum\limits_{i=1}^{T} K_{\mathrm{dis}}^{\mathrm{STO}} P_{\mathrm{dis}.i}^{\mathrm{STO}} X_{\mathrm{dis}.i}^{\mathrm{STO}} \\ F^{\mathrm{sto}} = F^{\mathrm{ACC}} + F^{\mathrm{TS}} + F^{\mathrm{CS}} \\ \mathrm{STO} = [\mathrm{ACC}, \mathrm{TS}, \mathrm{CS}] \end{cases} \tag{6}$$

where STO represents the variables associated with the energy storage devices, F^{STO} is the operating cost of the energy storage devices, $P^{\mathrm{STO}}_{\mathrm{cha}.i}$ and $P^{\mathrm{STO}}_{\mathrm{dis}.i}$ are the corresponding charging and discharging powers, $K^{\mathrm{STO}}_{\mathrm{cha}}$ and $K^{\mathrm{STO}}_{\mathrm{dis}}$ are the corresponding charging and discharging cost coefficients, and $X^{\mathrm{STO}}_{\mathrm{cha}.i}$ and $X^{\mathrm{STO}}_{\mathrm{dis}.i}$ are the states of charging and discharging, respectively, which are binary variables (0 or 1).

3.1.6. Cost of Compensating Shiftable Loads F^{sh}

Shiftable loads primarily include electrical, thermal, and cooling loads. Shifting these loads can affect user comfort and therefore requires compensation. Assuming that the compensation cost is only related to the shifted power, the cost, F^{shift}, for shiftable loads is given by:

$$\begin{cases} F^{\mathrm{SH}} = F^{\mathrm{SH}}_{\mathrm{cost}} P^{\mathrm{SH}}_{\mathrm{sum}} \sum\limits_{i \in T^{\mathrm{SH}}}^{T^{\mathrm{SH}}} X^{\mathrm{SH}}_i \\ F^{\mathrm{sh}} = F^{\mathrm{sh.e}} + F^{\mathrm{sh.h}} + F^{\mathrm{sh.c}} \\ \mathrm{SH} = [\mathrm{sh.e}, \mathrm{sh.h}, \mathrm{sh.c}] \end{cases} \tag{7}$$

where SH represents the variables associated with shiftable loads, F^{SH} is the compensation cost for shiftable loads, $F^{\mathrm{SH}}_{\mathrm{cost}}$ is the unit compensation price for shifting, $P^{\mathrm{SH}}_{\mathrm{sum}}$ denotes the corresponding shifted power, X^{SH}_i is the shifting state, which is a binary variable (0 or 1), and T^{SH} represents the corresponding shifting time period.

3.1.7. Cost of Compensating Transferable Loads F^{tran}

Transferable loads primarily include electrical loads. Transferring these loads can affect user comfort and thus requires compensation. The cost, F^{tran}, for transferable loads is given by:

$$F^{\mathrm{tran}} = F^{\mathrm{tran}}_{\mathrm{cost}} \cdot \sum_{i \in T^{\mathrm{tran}}}^{T^{\mathrm{tran}}} X^{\mathrm{tran}}_i P^{\mathrm{tran}}_i \tag{8}$$

where $F^{\mathrm{tran}}_{\mathrm{cost}}$ is the unit compensation price for transfer, P^{tran}_i denotes the transferred power, X^{tran}_i is the transfer state, which is a binary variable (0 or 1), and T^{tran} represents the transfer time period.

3.1.8. Cost of Compensating Curtailable Loads F^{cut}

Curtailable loads primarily include electrical, thermal, and cooling loads. Reducing these loads can impact user comfort, and therefore, requires compensation. Assuming that the compensation cost is only related to the reduced power, the compensation cost, F^{cut}, for curtailable loads is given by:

$$\begin{cases} F^{\mathrm{CUT}} = F^{\mathrm{CUT}}_{\mathrm{cost}} \sum\limits_{i \in T^{\mathrm{CUT}}}^{T^{\mathrm{CUT}}} K^{\mathrm{CUT}}_i P^{\mathrm{CUT}}_i X^{\mathrm{CUT}}_i \\ F^{\mathrm{cut}} = F^{\mathrm{cut.e}} + F^{\mathrm{cut.h}} + F^{\mathrm{cut.c}} \\ \mathrm{CUT} = [\mathrm{cut.e}, \mathrm{cut.h}, \mathrm{cut.c}] \end{cases} \tag{9}$$

where CUT represents the variables associated with curtailable loads, F^{CUT} is the compensation cost for curtailable loads, $F^{\mathrm{CUT}}_{\mathrm{cost}}$ is the unit compensation price for reduction, K^{CUT}_i is the reduction factor, P^{CUT}_i denotes the reduced power, X^{CUT}_i is the reduction state, which is a binary variable (0 or 1), and T^{CUT} represents the reduction time period.

3.2. Constraint Condition

3.2.1. Electricity Interconnection Line Constraints

The power purchased from and sold to the grid should not exceed the maximum allowable power limits of the grid and system interconnection lines. Additionally, the

interconnection lines cannot be in a state of purchasing and selling power simultaneously within the same time period. Therefore, the following constraints must be satisfied:

$$\begin{cases} 0 \le P_i^{\text{pur}} \le P_{\max}^{\text{link}} X_i^{\text{pur}} \\ 0 \le P_i^{\text{sell}} \le P_{\max}^{\text{link}} X_i^{\text{sell}} \\ X_i^{\text{pur}} \cdot X_i^{\text{sell}} = 0 \end{cases} \tag{10}$$

where $P_{\max}^{\text{link}}$ is the maximum allowable power limits, and X_i^{pur} and X_i^{sell} are binary variables indicating the transaction states for purchasing and selling power, respectively.

3.2.2. Distributed Generation Constraints

The output of wind turbines and photovoltaic systems in each time period should not exceed the maximum allowable output for that period. Therefore, the following constraints must be satisfied:

$$\begin{cases} 0 \le P_i^{\text{wind}} \le P_{\max,i}^{\text{wind}} \\ 0 \le P_i^{\text{pv}} \le P_{\max,i}^{\text{pv}} \end{cases} \tag{11}$$

where $P_{\max,i}^{\text{wind}}$ and $P_{\max,i}^{\text{pv}}$ are the maximum allowable outputs for wind turbines and photovoltaic systems, respectively.

3.2.3. Natural Gas System Equipment Constraints

The output of natural gas system equipment must not exceed the upper and lower limits, and it must meet the specified ramp-up and ramp-down rates. Therefore, the following constraints must be satisfied:

$$\begin{cases} P_{\min}^{\text{GAS}} X_i^{\text{GAS}} \le P_i^{\text{GAS}} \le P_{\max}^{\text{GAS}} X_i^{\text{GAS}} \\ \left| P_i^{\text{GAS}} - P_{i-1}^{\text{GAS}} \right| \le r^{\text{GAS}} \Delta t \\ \text{GAS} = [\text{GT}, \text{GB}, \text{FC}] \end{cases} \tag{12}$$

where $P_{\min}^{\text{GAS}}$ and $P_{\max}^{\text{GAS}}$ are the lower and upper output limits of the natural gas system equipment, respectively, X_i^{GAS} is the operational status, which is a binary variable (0 or 1), r^{GAS} is the maximum ramp rates, respectively, and Δt is the duration of the scheduling time interval.

3.2.4. Interconnection Equipment Constraints

The output of interconnection equipment between subsystems must remain within a reasonable range and must adhere to the specified ramp-up and ramp-down rates. Therefore, the following constraints must be satisfied:

$$\begin{cases} 0 \le P_i^{\text{LIA}} \le P_{\max}^{\text{LIA}} X_i^{\text{LIA}} \\ \left| P_i^{\text{LIA}} - P_{i-1}^{\text{LIA}} \right| \le r^{\text{LIA}} \Delta t \\ \text{LIA} = [\text{EB}, \text{EC}, \text{AC}] \end{cases} \tag{13}$$

where $P_{\max}^{\text{LIA}}$ is the maximum output limit for the interconnection equipment, X_i^{LIA} is the operational status, which is a binary variable (0 or 1), and r^{LIA} is the maximum ramp-up rate for the interconnection equipment.

3.2.5. Energy Storage Constraints

During the system optimization scheduling process, the energy storage device must meet the following requirements:

- The state of charge must remain within specified upper and lower limits to prevent overcharging or deep discharging.
- The device cannot be in both charging and discharging states simultaneously within the same time period.

- The state of charge at the beginning and end of the scheduling period must be consistent.
- The maximum charging and discharging power should not exceed 20% of the rated capacity to prevent excessive wear on the storage device.
- The number of charging and discharging cycles should be limited to extend the lifespan of the storage device.

$$\begin{cases} S_{\min}^{\mathrm{STO}} \le S_i^{\mathrm{STO}} \le S_{\max}^{\mathrm{STO}} \\ X_{\mathrm{cha}.i}^{\mathrm{STO}} X_{\mathrm{dis}.i}^{\mathrm{STO}} = 0 \\ S_0^{\mathrm{STO}} = S_{T^{\mathrm{STO}}}^{\mathrm{STO}} \\ 0 \le P_{\mathrm{cha}.i}^{\mathrm{STO}} \le 0.2 E^{\mathrm{STO}} X_{\mathrm{cha}.i}^{\mathrm{STO}} \\ 0 \le P_{\mathrm{dis}.i}^{\mathrm{STO}} \le 0.2 E^{\mathrm{STO}} X_{\mathrm{dis}.i}^{\mathrm{STO}} \\ \frac{1}{2} \sum_{t=1}^{T^{\mathrm{STO}}} \left| X_i^{\mathrm{cha}} - X_{i-1}^{\mathrm{cha}} \right| \le N_{\mathrm{cha}}^{\mathrm{STO}} \\ \frac{1}{2} \sum_{t=1}^{T^{\mathrm{STO}}} \left| X_i^{\mathrm{dis}} - X_{i-1}^{\mathrm{dis}} \right| \le N_{\mathrm{dis}}^{\mathrm{STO}} \\ \mathrm{STO} = [\mathrm{ACC}, \mathrm{TS}, \mathrm{CS}] \end{cases} \tag{14}$$

where S_i^{STO} represents the state of charge of the energy storage device; $S_{\max}^{\mathrm{STO}}$ and $S_{\min}^{\mathrm{STO}}$ are the maximum and minimum state of charge values, respectively; $X_{\mathrm{cha}.i}^{\mathrm{STO}}$ and $X_{\mathrm{dis}.i}^{\mathrm{STO}}$ represent the charging and discharging states, respectively, both of which are binary variables (0 or 1); S_0^{STO} and $S_{T^{\mathrm{STO}}}^{\mathrm{STO}}$ are the initial and final state of charge, respectively, E^{STO} is the rated capacity of the storage device; and $N_{\mathrm{cha}}^{\mathrm{STO}}$ and $N_{\mathrm{dis}}^{\mathrm{STO}}$ are the maximum number of charging and discharging cycles, respectively.

3.2.6. Shiftable Load Constraints

Shiftable loads can only be shifted once within the shiftable period; thus, they must satisfy:

$$\begin{cases} \sum_{i \in T^{\mathrm{SH}}}^{T^{\mathrm{SH}}} X_i^{\mathrm{SH}} = 1 \\ \mathrm{SH} = [\mathrm{sh.e}, \mathrm{sh.h}, \mathrm{sh.c}] \end{cases} \tag{15}$$

3.2.7. Transferable Load Constraints

Transferable loads must meet the following requirements:

- The power should remain within a reasonable range.
- The minimum duration should be restricted to prevent frequent starts and stops of external equipment.
- The total load power should remain unchanged before and after the transfer.

$$\begin{cases} X_i^{\mathrm{tran}} P_{\min}^{\mathrm{tran}} \le P_i^{\mathrm{tran}} X_i^{\mathrm{tran}} P_{\max}^{\mathrm{tran}} \\ T_{\min}^{\mathrm{tran}} (X_i^{\mathrm{tran}} - X_{i-1}^{\mathrm{tran}}) \le \sum_{t=i}^{i+T_{\min}^{\mathrm{tran}}-1} X_t^{\mathrm{tran}} \\ \sum_{i=1}^{T} X_i^{\mathrm{tran}} P_i^{\mathrm{tran}} = P_{\mathrm{sum}}^{\mathrm{tran}} \end{cases} \tag{16}$$

where $P_{\max}^{\mathrm{tran}}$ and $P_{\min}^{\mathrm{tran}}$ are the maximum and minimum allowable transfer values, respectively, $T_{\min}^{\mathrm{tran}}$ is the minimum duration for the transferable load, and $P_{\mathrm{sum}}^{\mathrm{tran}}$ is the total power of the transferable load.

3.2.8. Curtailable Load Constraints

Curtailable loads must meet the following requirements:

- The curtailment coefficient should remain within a reasonable range.

- The minimum continuous curtailment time should be restricted to prevent fluctuations in equipment operation.
- To consider user satisfaction, the maximum continuous curtailment time should be limited.
- To consider user experience, the maximum number of curtailments should be limited.

$$\begin{cases} X_i^{\text{tran}} P_{\min}^{\text{tran}} \le P_i^{\text{tran}} X_i^{\text{tran}} P_{\max}^{\text{tran}} \\ T_{\min}^{\text{tran}} (X_i^{\text{tran}} - X_{i-1}^{\text{tran}}) \le \sum_{t=i}^{i+T_{\min}^{\text{tran}}-1} X_t^{\text{tran}} \\ \sum_{i=1}^{T} X_i^{\text{tran}} P_i^{\text{tran}} = P_{\text{sum}}^{\text{tran}} \end{cases} \tag{17}$$

where $K_{\max,i}^{\text{CUT}}$ and $K_{\min,i}^{\text{CUT}}$ are the maximum and minimum curtailment coefficients, respectively, $T_{\max}^{\text{CUT}}$ and $T_{\min}^{\text{CUT}}$ are the maximum and minimum continuous curtailment times, respectively, and $N_{\max}^{\text{CUT}}$ is the maximum number of curtailments.

3.2.9. Power Balance Constraints

The power flowing into and out of an electrical bus must balance, and it should satisfy:

$$\begin{cases} (P_i^{\text{pur}} - P_i^{\text{sell}}) + P_i^{\text{wind}} + P_i^{\text{pv}} + P_i^{\text{GT.e}} + P_i^{\text{FC}} + (P_{\text{dis}.i}^{\text{ACC}} - P_{\text{cha}.i}^{\text{ACC}}) = P_i^{\text{EB.in}} + P_i^{\text{EC.in}} + P_i^{\text{load.e}} \\ P_i^{\text{load.e}} = P_i^{\text{base.e}} + P_i^{\text{sh.e}} + P_i^{\text{tran}} + P_i^{\text{cut.e}} \end{cases} \tag{18}$$

where $P_i^{\text{EB.in}}$ and $P_i^{\text{EC.in}}$ represent the electricity consumption power of the electric boiler and electric chiller, respectively, $P_i^{\text{load.e}}$ is the total electricity consumption power, and $P_i^{\text{base.e}}$ is the electricity consumption power of the base load.

The power flowing into and out of a thermal bus must balance, and it should satisfy:

$$\begin{cases} P_i^{\text{GT.h}} + P_i^{\text{EB}} + P_i^{\text{GB}} + (P_{\text{dis}.i}^{\text{TS}} - P_{\text{cha}.i}^{\text{TS}}) = P_i^{\text{AC.in}} + P_i^{\text{load.h}} \\ P_i^{\text{load.h}} = P_i^{\text{base.h}} + P_i^{\text{sh.h}} + P_i^{\text{cut.h}} \end{cases} \tag{19}$$

where $P_i^{\text{AC.in}}$ represents the heat consumption power of the absorption chiller, $P_i^{\text{load.h}}$ is the total heat consumption power, and $P_i^{\text{base.h}}$ is the heat consumption power of the load.

The power flowing into and out of a cooling bus must balance, and it should satisfy:

$$\begin{cases} P_i^{\text{AC}} + P_i^{\text{EC}} + (P_{\text{dis}.i}^{\text{CS}} - P_{\text{cha}.i}^{\text{CS}}) = P_i^{\text{load.c}} \\ P_i^{\text{load.c}} = P_i^{\text{base.c}} + P_i^{\text{sh.c}} + P_i^{\text{cut.c}} \end{cases} \tag{20}$$

where $P_i^{\text{load.c}}$ represents the total cooling power consumption, and $P_i^{\text{base.c}}$ is the cooling power consumption of the base load.

4. Day-Ahead Two-Layer Optimization Strategy for IES

Based on the time-scale characteristics of energy dynamics, a two-layer rolling optimization model for intra-day scheduling is proposed, as illustrated in Figure 2. This model divides the intra-day scheduling into an upper-layer thermal and cooling energy scheduling model and a lower-layer electrical energy scheduling model. The upper-layer model is designed to handle the slow response rate of thermal and cooling energy power fluctuations, while the lower-layer model controls the rapid response rate of electrical power fluctuations. This process uses the day-ahead scheduling plan as a basis and incrementally adjusts the day-ahead plan values by rolling updates of distributed generation outputs and ultra-short-term load forecasts, thereby fine-tuning the outputs of controllable components in the system.

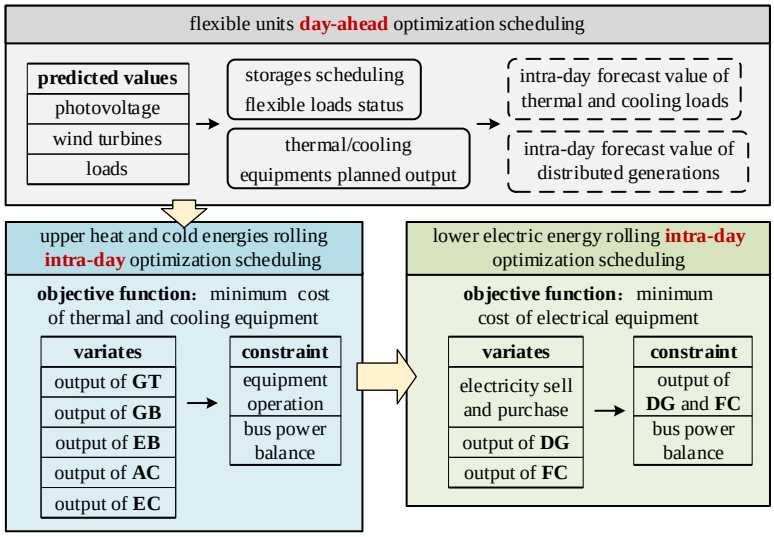

Figure 2. Intra-day two-layer scheduling strategy diagram.

Considering the complexity of load switching and operation, the operational states of curtailable loads, shiftable loads, and transferable loads in the intra-day plan are predetermined by the day-ahead plan. Due to the frequent power fluctuations in the intra-day operation plan and the fact that energy storage devices are generally at their maximum number of charge/discharge cycles as per the day-ahead plan, energy storage devices do not participate in the intra-day scheduling plan.

The fluctuation of cold and heat load is greatly affected by climate, season, daily change, and other factors. For example, in summer, the temperature difference between indoor and outdoor is large, and the air conditioning system needs more cooling capacity to maintain the indoor temperature, so the cooling load is large; in winter, more heat is needed to maintain the indoor temperature, and the heat load is large. Electrical load refers to the total power consumed by all users connected to the system distribution network and the power used to compensate for the loss of all parts of the grid (transformers, converters, and transmission lines). The size of the electricity load depends on the user's electrical equipment power, electricity time, and power supply capacity of the power system and other factors. In summary, although the cold and heat load and the electric load have certain similarities in the time scale of the fluctuation, there are differences in the application of the specific load forecasting time scale. The fluctuation of the power load is more frequent, and the change of the daily load curve directly affects the operation and economy of the power system. Compared with the power load, the time scale of the cold and heat load fluctuation may pay more attention to the long-term impact of planning and design. Therefore, this paper chooses the time scale of electric load for 15 min and cold and heat load for 1 h.

The intra-day scheduling time-domain control strategy is illustrated in Figure 3. For the upper-layer thermal and cooling energy scheduling model, the time interval is $\Delta t_1 = 1$ h. This model generates the scheduling plan for the prediction and control domains. Based on the optimization results, the scheduling plan for the control domain is executed and forwarded to the lower-layer electrical energy scheduling model, awaiting its scheduling completion instructions. The prediction and control domains are then rolled forward to the next time interval, and the process is repeated.

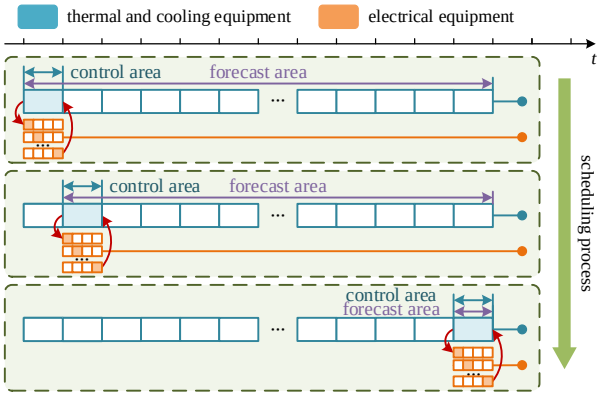

Figure 3. Intra-day scheduling time-domain control strategy diagram.

For the lower-layer electrical energy scheduling model, the time interval is $\Delta t_2 = 15$ min. This model waits for the scheduling plan instructions from the control domain of the upper-layer model and determines the optimization scheduling strategy for the electrical system at this layer. Given the shorter scheduling time window at this layer, after dynamic rolling optimization through multiple time windows, the rolling optimization is stopped when the lower-layer scheduling time window overlaps with the end time of the upper-layer time window. The lower layer then sends a scheduling completion instruction to the upper layer, which repeats the scheduling and execution for the next time window.

4.1. Upper-Layer Thermal and Cooling Energy Scheduling Model

4.1.1. Objective Function

The upper-layer scheduling model mainly focuses on the total cost of scheduling thermal and cooling energy equipment. The objective function is:

$$\min \Delta F_{\text{up}} = \sum_{j=i+1}^{i+2} \begin{array}{l} \Delta F_j^{\text{GT}} + \Delta F_j^{\text{GB}} + \Delta F_j^{\text{EB}} + \Delta F_j^{\text{EC}} + \\ \Delta F_j^{\text{AC}} - \Delta F_j^{\text{GT.e}} + \Delta F_j^{\text{EB.in}} + \Delta F_j^{\text{EC.in}} \end{array} \tag{21}$$

where ΔF_j^{GT}, ΔF_j^{GB}, ΔF_j^{EB}, ΔF_j^{EC}, and ΔF_j^{AC} represent the incremental operating costs of the gas turbine, gas boiler, electric boiler, electric chiller, and absorption chiller, respectively. The calculation methods for these costs are consistent with those used in the day-ahead scheduling; $\Delta F_j^{\text{GT.e}}$ represents the incremental electricity revenue from the gas turbine, and $\Delta F_j^{\text{EB.in}}$ and $\Delta F_j^{\text{EC.in}}$ represent the incremental electricity consumption costs for the electric boiler and electric chiller during the intra-day phase, respectively. The calculation methods for these are as follows:

$$\begin{cases} \Delta F_j^{\text{GT.e}} = K_{\text{pur}}^{\text{mean}} \Delta P_j^{\text{GT.e}} \\ \Delta F_j^{\text{EB.in}} = K_{\text{pur}}^{\text{mean}} \Delta P_j^{\text{EB.in}} \\ \Delta F_j^{\text{EC.in}} = K_{\text{pur}}^{\text{mean}} \Delta P_j^{\text{EC.in}} \end{cases} \tag{22}$$

where $K_{\text{pur}}^{\text{mean}}$ is the average purchase electricity price, $K_{\text{pur}}^{\text{mean}} = \frac{\sum_{i=1}^{24} K_i^{\text{pur}}}{24}$, $\Delta P_j^{\text{GT.e}}$ is the incremental electricity generation power of the gas turbine, and $\Delta P_j^{\text{EB.in}}$ and $\Delta P_j^{\text{EC.in}}$ are the incremental electricity consumption powers of the electric boiler and electric chiller, respectively.

4.1.2. Constraint Condition

1. Thermal and cooling energy equipment operation constraints

After adjusting the power, the output of each device must not exceed its upper and lower limits. Therefore, the following constraints should be satisfied:

$$\begin{cases} P_{\min}^{GT} \cdot X_j^{GT} \le P_j^{GT} + \Delta P_j^{GT} \le P_{\max}^{GT} \cdot X_j^{GT} \\ P_{\min}^{GB} \cdot X_j^{GB} \le P_j^{GB} + \Delta P_j^{GB} \le P_{\max}^{GB} \cdot X_j^{GB} \\ 0 \le P_j^{EB} + \Delta P_j^{EB} \le P_{\max}^{EB} \\ 0 \le P_j^{EC} + \Delta P_j^{EC} \le P_{\max}^{EC} \\ 0 \le P_j^{AC} + \Delta P_j^{AC} \le P_{\max}^{AC} \end{cases} \tag{23}$$

where P_j^{GT}, P_j^{GB}, P_j^{EB}, P_j^{EC}, and P_j^{AC} represent the day-ahead scheduling output for the gas turbine, gas boiler, electric boiler, electric chiller, and absorption chiller, respectively, and ΔP_j^{GT}, ΔP_j^{GB}, ΔP_j^{EB}, ΔP_j^{EC}, and ΔP_j^{AC} represent the corresponding output increments.

The output of each device should also meet the up and down ramp rate constraints. Therefore, the following conditions should be satisfied:

$$\begin{cases} \left|(P_j^{GT} + \Delta P_j^{GT}) - (P_{j-1}^{GT} + \Delta P_{j-1}^{GT})\right| \le r^{GT}\Delta t_1 \\ \left|(P_j^{GB} + \Delta P_j^{GB}) - (P_{j-1}^{GB} + \Delta P_{j-1}^{GB})\right| \le r^{GB}\Delta t_1 \\ \left|(P_j^{EB} + \Delta P_j^{EB}) - (P_{j-1}^{EB} + \Delta P_{j-1}^{EB})\right| \le r^{EB}\Delta t_1 \\ \left|(P_j^{AC} + \Delta P_j^{AC}) - (P_{j-1}^{AC} + \Delta P_{j-1}^{AC})\right| \le r^{AC}\Delta t_1 \\ \left|(P_j^{EC} + \Delta P_j^{EC}) - (P_{j-1}^{EC} + \Delta P_{j-1}^{EC})\right| \le r^{EC}\Delta t_1 \end{cases} \tag{24}$$

2. Thermal bus power balance

According to the thermal bus power balance, the following condition should be satisfied:

$$\begin{cases} \Delta P_j^{GT.h} + \Delta P_j^{EB} + \Delta P_j^{GB} = \Delta P_j^{AC.in} + \Delta P_j^{load.h} \\ \Delta P_j^{load.h} = \Delta P_j^{base.h} + \Delta P_j^{sh.h} + \Delta P_j^{cut.h} \end{cases} \tag{25}$$

where $\Delta P_j^{GT.h}$ represents the increment in the heat output of the gas turbine, $\Delta P_j^{AC.in}$ represents the increment in the heat consumption of the absorption chiller, and $\Delta P_j^{load.h}$ represents the increment in the thermal load power required based on short-term forecasting compared to the day-ahead forecast.

3. Cooling bus power balance

According to the cooling bus power balance, the following condition should be satisfied:

$$\begin{cases} \Delta P_j^{AC} + \Delta P_j^{EC} = \Delta P_j^{load.c} \\ \Delta P_i^{load.c} = \Delta P_i^{base.c} + \Delta P_i^{sh.c} + \Delta P_i^{cut.c} \end{cases} \tag{26}$$

where $\Delta P_j^{load.c}$ represents the increment in the cooling load power required based on short-term forecasting compared to the day-ahead forecast.

4.2. Lower-Level Electrical Energy Scheduling Model

4.2.1. Lower-Level Electrical Energy Scheduling Model Objective Function

In the lower-level scheduling model, the primary focus is on the incremental total cost of electrical energy equipment scheduling. The objective function is:

$$\min \Delta F_{low} = \sum_{j=k+1}^{k+4} \Delta F_j^{grid} + \Delta F_j^{DG} + \Delta F_j^{FC} + 0.25 K_{pur}^{mean} (\Delta P_j^{EB.in} + \Delta P_j^{EC.in} - \Delta P_j^{GT.e}) \tag{27}$$

where ΔF_j^{grid} represents the incremental cost of purchasing electricity from the grid, ΔF_j^{DG} denotes the incremental operating cost of distributed generation sources, and ΔF_j^{FC} indicates the incremental cost of fuel cells. The calculations for ΔF_j^{grid}, ΔF_j^{DG}, and ΔF_j^{FC} are consistent with those used in the day-ahead scheduling.

4.2.2. Lower-Level Electrical Energy Scheduling Model Objective Function Component

1. Power interconnection line constraints between the grid and the system

After changes in the system's power purchase and sale, they must still remain within the maximum allowable power limits of the interconnection lines between the grid and the system. Additionally, the interconnection lines cannot be in both purchase and sale modes simultaneously within the same time period. Therefore, the following constraints must be satisfied:

$$\begin{cases} 0 \le P_j^{\text{pur}} + \Delta P_j^{\text{pur}} \le P_{\max}^{\text{link}} \cdot \Delta X_j^{\text{pur}} \\ 0 \le P_j^{\text{sell}} + \Delta P_j^{\text{sell}} \le P_{\max}^{\text{link}} \cdot \Delta X_j^{\text{sell}} \\ \Delta X_j^{\text{pur}} \cdot \Delta X_j^{\text{sell}} = 0 \end{cases} \tag{28}$$

where ΔP_j^{pur} and ΔP_j^{sell} represent the increments in power purchase and sale, respectively, and ΔX_j^{pur} and ΔX_j^{sell} denote the transaction states for power purchase and sale, respectively.

2. Distributed generation constraints

After power adjustment, the output of wind turbines and photovoltaic units should not exceed the maximum allowable output for each period. Therefore, the following constraints must be met:

$$\begin{cases} 0 \le P_j^{\text{wind}} + \Delta P_j^{\text{wind}} \le \widetilde{P}_{\max,j}^{\text{wind}} \\ 0 \le P_j^{\text{pv}} + \Delta P_j^{\text{pv}} \le \widetilde{P}_{\max,j}^{\text{pv}} \end{cases} \tag{29}$$

where P_j^{wind} and P_j^{pv} represent the output of wind turbines and photovoltaic units from the day-ahead scheduling plan, ΔP_j^{wind} and ΔP_j^{pv} denote the output increments for wind turbines and photovoltaic units, and $\widetilde{P}_{\max,j}^{\text{wind}}$ and $\widetilde{P}_{\max,j}^{\text{pv}}$ refer to the intra-day scheduling forecast values for wind turbines and photovoltaic units, respectively.

3. Fuel Cell

After adjusting the power, the output of the fuel cell should not exceed its upper and lower limits and must meet the maximum ramp-up and ramp-down rates. The following constraints should be satisfied:

$$\begin{aligned} &P_{\min}^{\text{FC}} \Delta X_j^{\text{FC}} \le P_j^{\text{FC}} + \Delta P_j^{\text{FC}} \le P_{\max}^{\text{FC}} \Delta X_j^{\text{FC}} \\ &\left| (P_j^{\text{FC}} + \Delta P_j^{\text{FC}}) - (P_{j-1}^{\text{FC}} + \Delta P_{j-1}^{\text{FC}}) \right| \le r^{\text{FC}} \Delta t_2 \end{aligned} \tag{30}$$

where P_j^{FC} represents the fuel cell's scheduled output from the day-ahead plan, ΔP_j^{FC} denotes the fuel cell output increment, ΔX_j^{FC} is the operational state of the fuel cell, and Δt_2 = 15 min.

4. Power Balance for Electrical Bus

According to the power balance for the electrical bus, the following must be satisfied:

$$\begin{cases} (\Delta P_j^{\text{pur}} - \Delta P_j^{\text{sell}}) + \Delta P_j^{\text{wind}} + \Delta P_j^{\text{pv}} + \Delta P_j^{\text{FC}} + \\ \Delta P_j^{\text{GT.e}} = \Delta P_j^{\text{EB.in}} + \Delta P_j^{\text{EC.in}} + \Delta P_j^{\text{load.e}} \\ \Delta P_i^{\text{load.e}} = \Delta P_i^{\text{base.e}} + \Delta P_i^{\text{sh.e}} + \Delta P_i^{\text{tran}} + \Delta P_i^{\text{cut.e}} \end{cases} \tag{31}$$

where ΔP_j^{load} is the difference between the short-term and day-ahead forecasts of electrical load in the j-th time period.

5. Case Study Analysis

5.1. Integrated Energy System Parameter Settings

The day-ahead and intra-day output prediction curves of photovoltaic and wind turbines in the integrated energy system are shown in Figures 4 and 5.

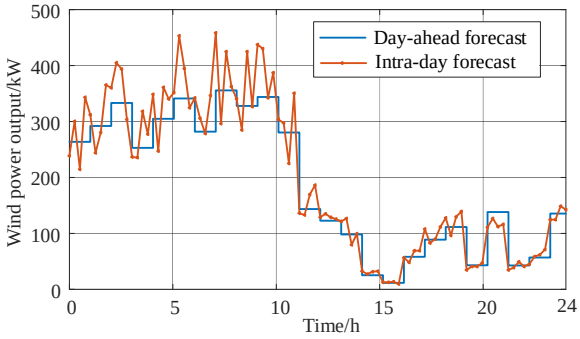

Figure 4. Day-ahead and intra-day output prediction curves of wind turbines.

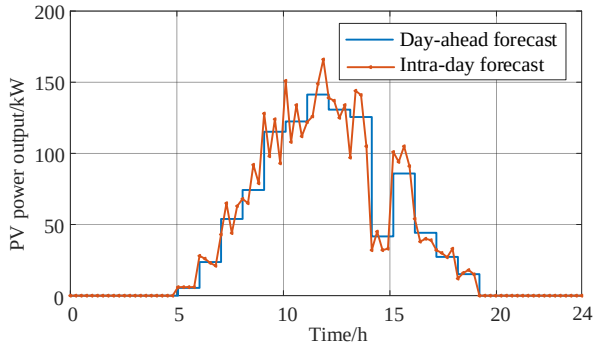

Figure 5. Day-ahead and intra-day output prediction curves of PV supply.

The user-side load includes the electrical load, thermal load, and cooling load. The electrical load includes basic electrical load, shiftable electrical load, transferable electrical load, and curtailable electrical load, and its day-ahead prediction value is shown in Figure 6.

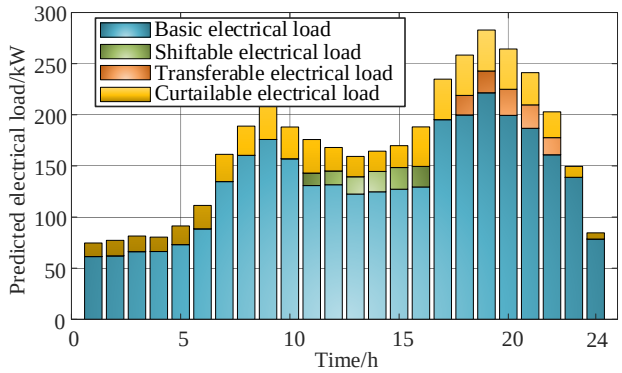

Figure 6. Day-ahead forecast value of electric load.

The user-side heat load includes the basic heat load, shiftable heat load, and curtailable heat load, and its day-ahead predicted value is shown in Figure 7.

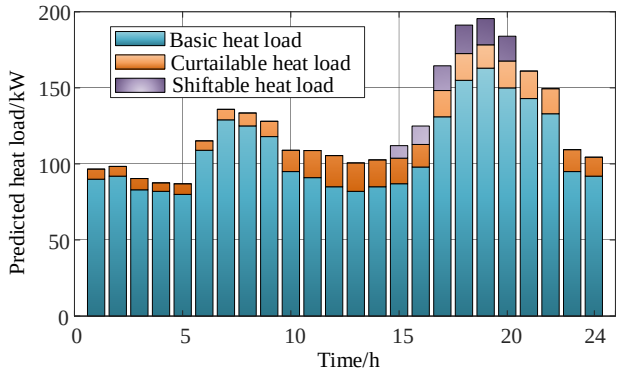

Figure 7. Day-ahead forecast value of heat load.

The user-side cold load includes the basic cold load, shiftable cold load, and cuttable cold load, and its day-ahead predicted value is shown in Figure 8.

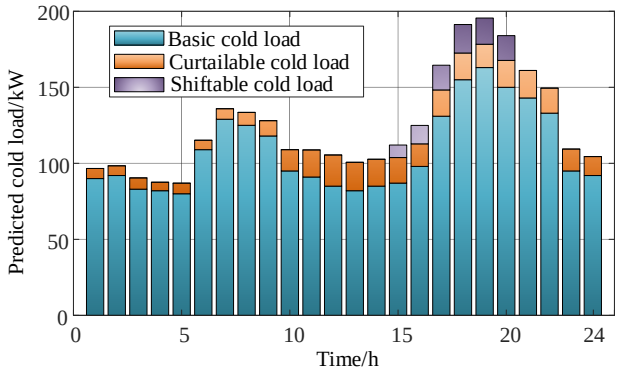

Figure 8. Day-ahead forecast value of cold load.

In the intra-day plan, the switching state of the load that can be reduced, the running state of the shiftable load, and the transferable load are given by the day-ahead plan and no longer optimized. The intra-day electric load forecasting deviation curve is shown in Figure 9.

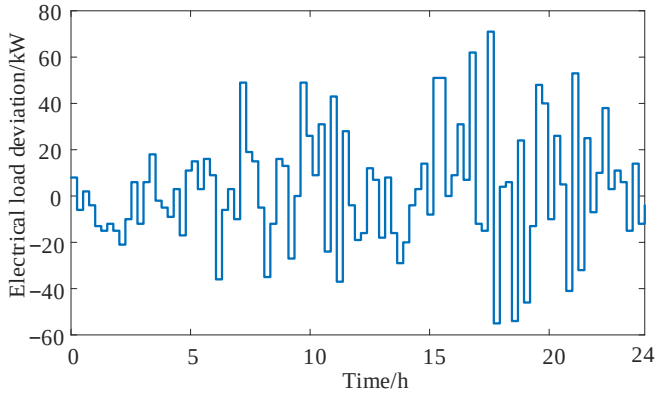

Figure 9. The intra-day electric load forecasting deviation.

The fluctuation of the cold and heat load is slow. In the intra-day scheduling, the prediction time scale of the cold and heat load is consistent with that of the day-ahead scheduling, and only the fluctuation of the value is considered. The intra-day and day-ahead difference of the cold and heat load is shown in Figure 10.

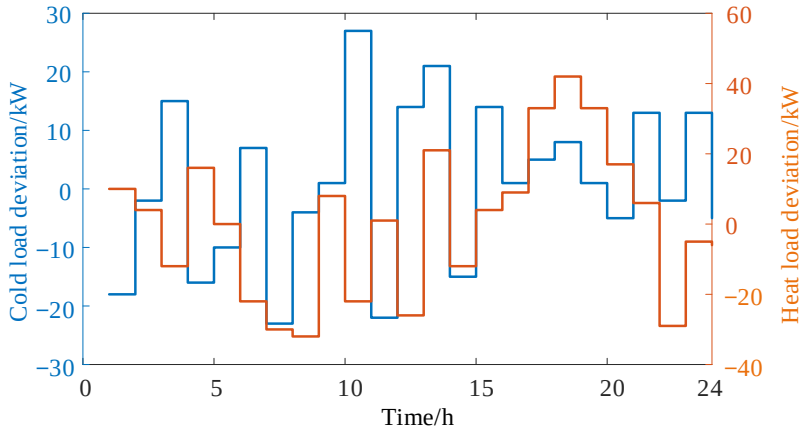

Figure 10. The intra-day and day-ahead difference of cold and heat load.

In this paper, the fuel cell generates electric energy by burning natural gas. The relevant parameters are the upper limit of power of 100 kW, the lower limit of power of 40 kW, the maximum uplink of 40 kW/h, the maximum downlink of 40 kW/h, and the operating cost of 0.4 ¥/kW. The price of natural gas is 3.23 ¥/m^3, the calorific value of combustion is 9.78 MJ/m^3, and the price of electricity purchase and sale is shown in Figure 11.

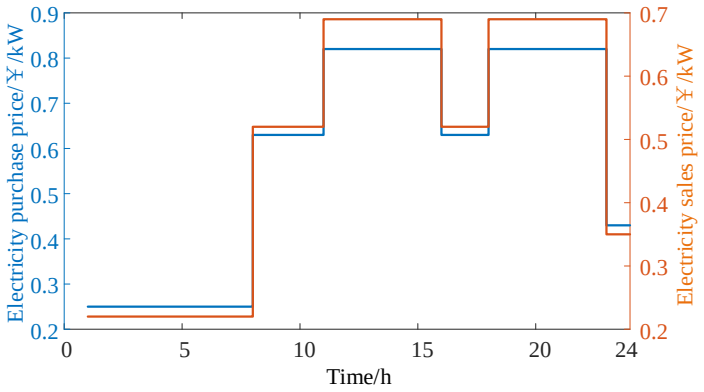

Figure 11. The price of electricity purchase and sale.

5.2. Day-Ahead Optimal Operation Results of Integrated Energy System

In this paper, Cplex 12.9 solver is used to solve the proposed optimization model. By solving the day-ahead optimization model of the integrated energy system, the optimal output of power equipment such as wind turbines, photovoltaics, and energy storage is shown in Figure 12, the optimal output of thermal components such as GB, GT, and EB is shown in Figure 13, and the optimal output of AC, EC, and cold storage tanks is shown in Figure 14. Through the optimal output of power components, thermal components, and cooling components, the demand of the power load, thermal load, and cooling load in the integrated energy system is met, and the reliability of the energy supply in the integrated energy system is guaranteed.

The shiftable electric load, transferable electric load, and curtailable electric load before and after the optimization of the electric load are shown in Figures 15–17. The peak value of the electric load before optimization is 301.069 kW, and the valley value is 80.020 kW. The peak value after optimization is 249.830 kW, and the valley value is 102.510 kW. It can be seen that through the demand side response, the overall load distribution is more gentle, the problem of the large peak valley difference is improved, and the significant peak shifting, peak clipping, and valley filling are realized.

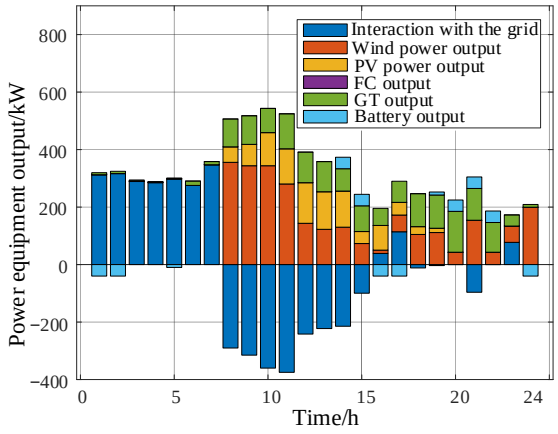

Figure 12. The optimal output of power equipment.

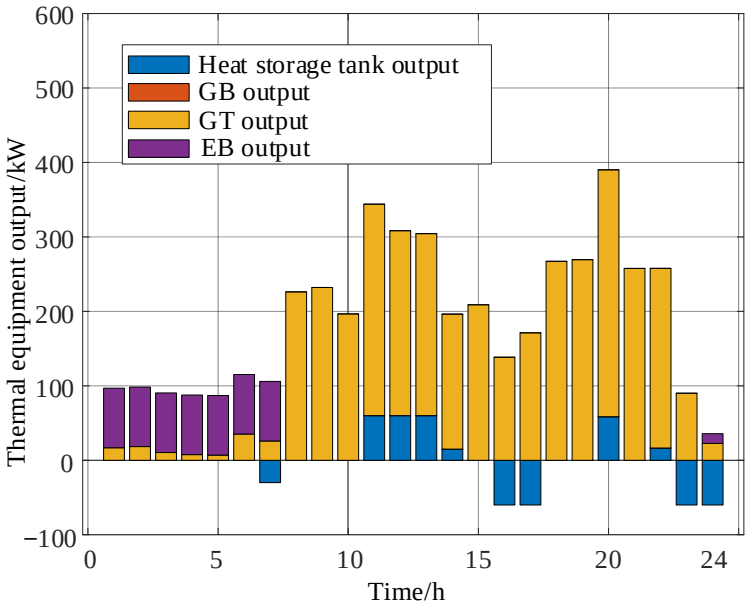

Figure 13. The optimal output of thermal equipment.

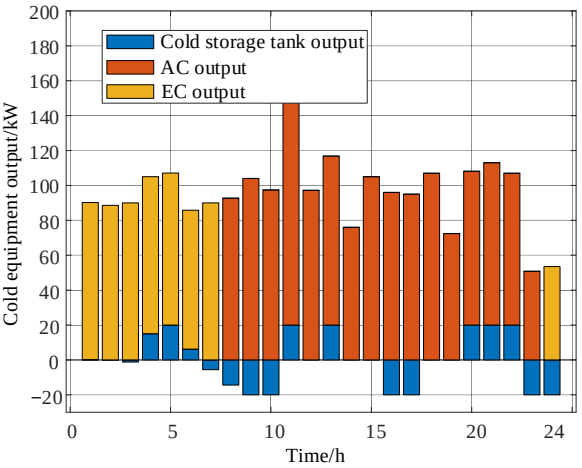

Figure 14. The optimal output of cold equipment.

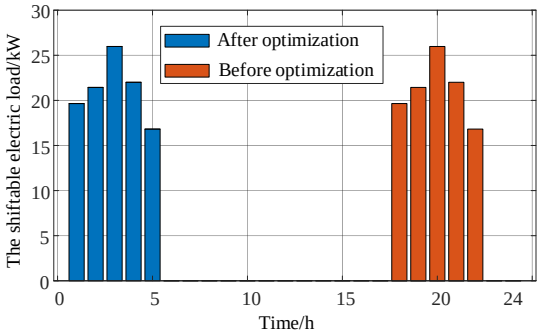

Figure 15. The shiftable electric load before and after optimization.

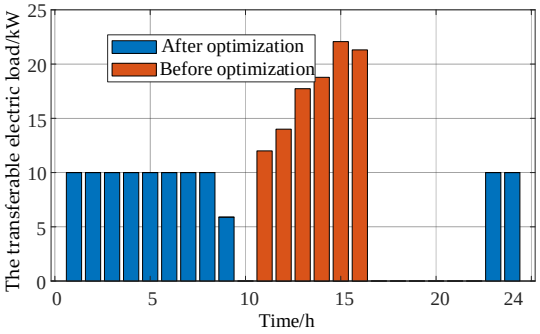

Figure 16. The transferable electric load before and after optimization.

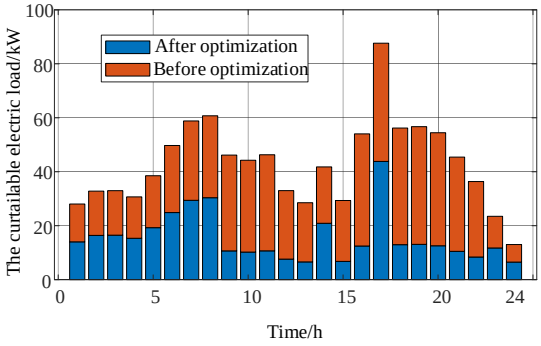

Figure 17. The curtailable electric load before and after optimization.

The shiftable heat load and the curtailable heat load before and after optimization are shown in Figures 18 and 19. The peak value of the heat load before optimization is 195.580 kW, and the valley value is 86.970 kW. After optimization, the peak value is 184.590 kW, and the valley value is 96.521 kW. It can be seen that the overall load distribution is more gentle through the demand side response.

The shiftable cold load and the curtailable cold load before and after optimization are shown in Figures 20 and 21. The peak cooling load before optimization is 130 kW, and the valley value is 67 kW. The peak cooling load after optimization is 124 kW, and the valley value is 75.100 kW. It can be seen that the overall cooling load distribution is more gentle through the demand side response.

In this paper, two sets of specific scenarios are set to verify the advantages of the proposed strategy in the economic operation of the integrated energy system. The specific settings of the scenarios are as follows:

Scenario 1: The flexible load is not involved in the scheduling, and only all the controllable components in the system are considered to participate in the day-ahead scheduling.

Scenario 2: Flexible electric load, flexible heat load, and flexible cooling load are considered to participate in day-ahead scheduling, and all controllable components in the system participate in day-ahead scheduling.

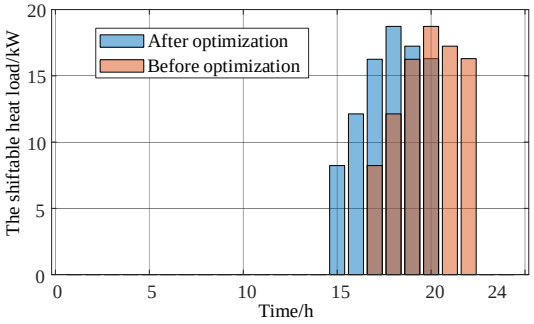

Figure 18. The shiftable heat load before and after optimization.

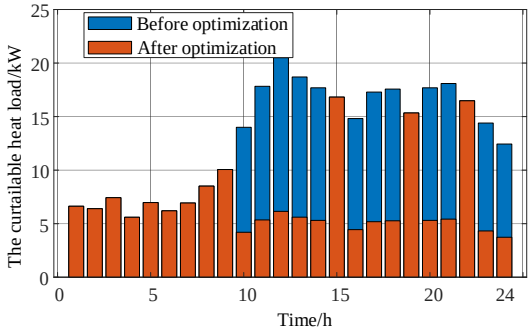

Figure 19. The curtailable heat load before and after optimization.

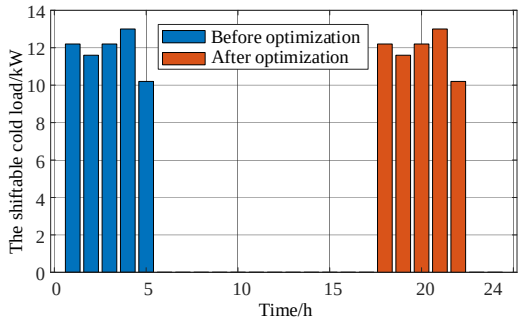

Figure 20. The shiftable cold load before and after optimization.

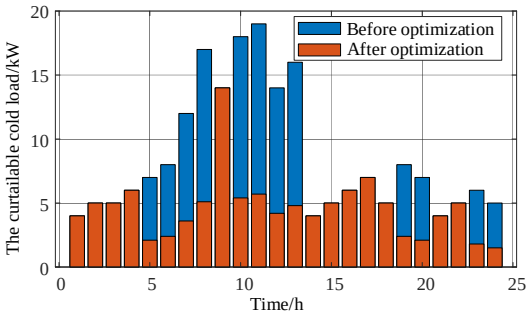

Figure 21. The curtailable cold load before and after optimization.

In the two groups of scenarios, the total operation cost, operation and maintenance cost, and power purchase cost of the integrated energy system are shown in Table 1. It can

be seen that under the strategy proposed in this paper, the flexible load participates in the demand side response of the integrated energy system, which significantly reduces the operation cost of the integrated energy system.

Table 1. The cost of the integrated energy system.

Scenario	Operation Cost (¥)	Power Purchase Cost (¥)	Total Operation Cost (¥)
Scenario 1	1869.0	1362.6	3231.6
Scenario 2	1901.0	1053.4	2954.4

5.3. Results of Intra-Day Optimal Operation of Integrated Energy System

By solving the intra-day optimization model of the integrated energy system, the optimal incremental output of power components such as wind turbines, photovoltaics, and energy storage is shown in Figure 22; the optimal incremental output of thermal components such as GB, GT, and EB is shown in Figure 23; and the optimal incremental output of AC, EC, and cold storage tanks is shown in Figure 24. Under the two-stage comprehensive energy system optimization model, the total cost of the system is 2947.2 ¥, which is lower than the total cost of Scenario 2. Meanwhile, through intra-day two-stage rolling scheduling, the impact of load forecasting and renewable energy day-ahead forecasting errors on the optimal operation of the integrated energy system can be effectively solved, and the internal energy supply reliability of the integrated energy system can be improved under the premise of ensuring the overall economy of the integrated energy system.

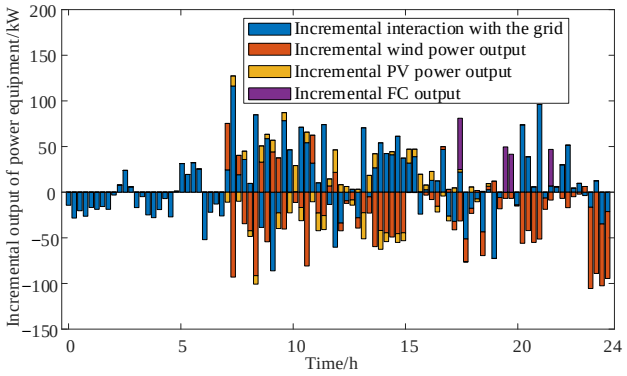

Figure 22. Incremental output of power equipment.

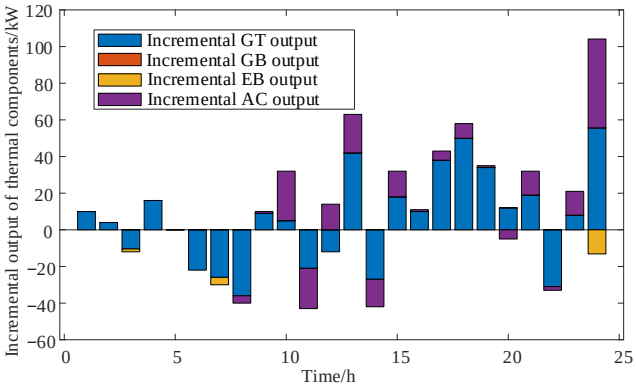

Figure 23. Incremental output of thermal equipment.

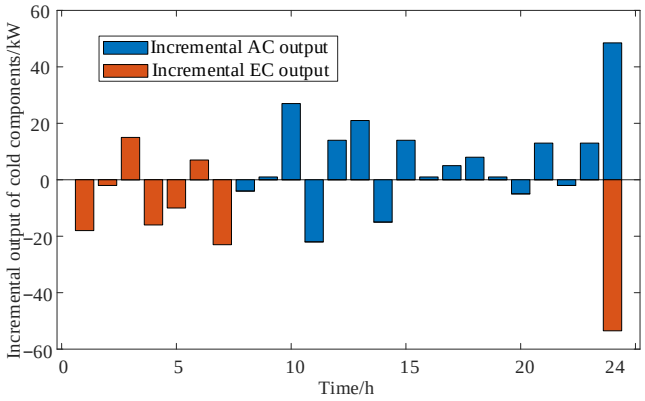

Figure 24. Incremental output of cold equipment.

6. Conclusions

This paper addresses the intra-day scheduling problem of IESs by proposing a two-layer optimization scheduling strategy that considers dynamic time intervals to enhance system efficiency and operational economy. The conclusions are as follows:

(1) Two-layer scheduling model: The intra-day scheduling is divided into an upper-layer thermal and cooling energy scheduling model and a lower-layer electrical energy scheduling model. The upper-layer model handles slow dynamics, while the lower-layer model addresses fast dynamics, enabling coordinated optimization of energy flows and improving overall system efficiency.

(2) Dynamic scheduling instruction periods: The method dynamically adjusts scheduling instruction periods to handle the time-delay characteristics of each subsystem, ensuring precise and real-time scheduling. This enhances the operational stability and economic performance of the IES.

(3) Effectiveness and superiority validated: Case studies demonstrate that the proposed method effectively coordinates the operating states of various devices within the IES, improving stability and economic performance. The model adapts well to energy type fluctuations and optimizes energy utilization, proving its practicality and superiority.

Author Contributions: Conceptualization, S.Z. and H.Z.; methodology, H.Z.; software, H.Z.; validation, F.W., B.Z. and Q.K.; formal analysis, H.Z.; investigation, H.Z.; resources, C.L.; data curation, C.L.; writing—original draft preparation, S.Z.; writing—review and editing, H.Z.; visualization, H.Z.; supervision, H.Z.; project administration, F.W.; funding acquisition, S.Z. All authors have read and agreed to the published version of the manuscript.

Funding: This work was by the State Grid Beijing Electric Power Company (5700-202311602A-3-2-ZN).

Data Availability Statement: Data is unavailable due to privacy or ethical restrictions.

Conflicts of Interest: The authors declare that they have no known competing financial interests or personal relationships that could have appeared to influence the work reported in this paper.

Nomenclature

IES	integrated Energy System	DG	distributed generations
GT	gas turbines	GB	gas boilers
FC	fuel cells	EB	electric boilers
EC	electric chillers	F^{grid}	system's electricity purchasing cost
P_i^{pur}, P_i^{sell}	power transactions with the grid	K_i^{pur}, K_i^{sell}	power transaction cost with the grid
F^{DG}	operating cost of DG	P_i^{wind}, P_i^{pv}	power output from DG
K^{wind}, K^{pv}	operating cost coefficients for DG	F^{gas}	total operating cost of GAS

GAS	variables with natural gas system	F^{GAS}	cost of natural gas system equipment
P_i^{GAS}	gas system equipment output	$P_i^{\mathrm{GT.e}}$	gas turbine electrical output
$P_i^{\mathrm{GT.h}}$	gas turbine thermal output	V_i^{GAS}	corresponding gas purchase quantity
K^{gas}	unit price of natural gas	K^{GAS}	operating cost coefficient of GAS
LIA	variables with interconnection devices	F^{lia}	total operating cost of LIA
F^{LIA}	operating cost of LIA	P_i^{LIA}	corresponding output of LIA
K^{LIA}	operating cost coefficient of LIA	STO	variables with energy storage devices
F^{sto}	total operating cost of STO	F^{STO}	operating cost of STO
$P_{\mathrm{cha}.i}^{\mathrm{STO}}$, $P_{\mathrm{dis}.i}^{\mathrm{STO}}$	charge and discharge powers of STO	$K_{\mathrm{cha}}^{\mathrm{STO}}$, $K_{\mathrm{dis}}^{\mathrm{STO}}$	cost coefficient of STO
$X_{\mathrm{cha}.i}^{\mathrm{STO}}$, $X_{\mathrm{dis}.i}^{\mathrm{STO}}$	states of charging and discharging	SH	variables with shiftable loads
F^{sh}	cost of compensating shiftable loads	F^{SH}	compensation cost for shiftable loads
$F_{\mathrm{cost}}^{\mathrm{SH}}$	unit compensation price for shifting	$P_{\mathrm{sum}}^{\mathrm{SH}}$	corresponding shifted power
X_i^{SH}	shifting state	T^{SH}	corresponding shifting time period
F^{tran}	cost of transferable loads	$F_{\mathrm{cost}}^{\mathrm{tran}}$	unit compensation price for transfer
P_i^{tran}	transferred power	X_i^{tran}	transfer state
T^{tran}	transfer time period	F^{cut}	cost of compensating curtailable load
CUT	variables with curtailable loads	F^{CUT}	cost for curtailable loads
$F_{\mathrm{cost}}^{\mathrm{CUT}}$	unit compensation price for reduction	K_i^{CUT}	reduction factor
P_i^{CUT}	reduced power	X_i^{CUT}	reduction state
T^{CUT}	reduction time period	$P_{\mathrm{max}}^{\mathrm{link}}$	maximum allowable power limits
X_i^{pur}, X_i^{sell}	transaction states for grid power	$P_{\mathrm{max},i}^{\mathrm{wind}}$, $P_{\mathrm{max},i}^{\mathrm{pv}}$	maximum allowable outputs for DG
$P_{\mathrm{min}}^{\mathrm{GAS}}$, $P_{\mathrm{max}}^{\mathrm{GAS}}$	output limits of GAS	X_i^{GAS}	operational status
r^{GAS}	maximum ramp rates	Δt	duration of the time interval
$P_{\mathrm{max}}^{\mathrm{LIA}}$	maximum output limit for LIA	X_i^{LIA}	operational status
r^{LIA}	maximum ramp-up rate for LIA	S_i^{STO}	state of charge of STO
$S_{\mathrm{max}}^{\mathrm{STO}}$, $S_{\mathrm{min}}^{\mathrm{STO}}$	state of charge values	$X_{\mathrm{cha}.i}^{\mathrm{STO}}$, $X_{\mathrm{dis}.i}^{\mathrm{STO}}$	charging and discharging states
S_0^{STO}, $S_{T^{\mathrm{STO}}}^{\mathrm{STO}}$	initial and final state of charge	E^{STO}	rated capacity of the storage device
$N_{\mathrm{cha}}^{\mathrm{STO}}$, $N_{\mathrm{dis}}^{\mathrm{STO}}$	maximum number of charging and discharging cycles	$P_{\mathrm{max}}^{\mathrm{tran}}$, $P_{\mathrm{min}}^{\mathrm{tran}}$	maximum and minimum allowable transfer values
$T_{\mathrm{min}}^{\mathrm{tran}}$	minimum duration for the transferable load	$P_{\mathrm{sum}}^{\mathrm{tran}}$	total power of the transferable load
$K_{\mathrm{max}.i}^{\mathrm{CUT}}$, $K_{\mathrm{min}.i}^{\mathrm{CUT}}$	maximum and minimum curtailment coefficients	$T_{\mathrm{max}}^{\mathrm{CUT}}$, $T_{\mathrm{min}}^{\mathrm{CUT}}$	maximum and minimum continuous curtailment times
$N_{\mathrm{max}}^{\mathrm{CUT}}$	maximum number of curtailments	$P_i^{\mathrm{EB.in}}$, $P_i^{\mathrm{EC.in}}$	consumption power of EB and EC
$P_i^{\mathrm{load.e}}$	total electricity consumption power	$P_i^{\mathrm{base.e}}$	consumption power of the base load
$P_i^{\mathrm{load.h}}$	heat consumption power of AC		total heat consumption power
$P_i^{\mathrm{base.h}}$	heat consumption power of the load	$P_i^{\mathrm{load.c}}$	total cooling power consumption
$P_i^{\mathrm{base.c}}$	cooling power consumption of the base load	$\Delta F_j^{\mathrm{GT.e}}$	incremental electricity revenue from GT
$K_{\mathrm{pur}}^{\mathrm{mean}}$	average purchase electricity price	$\Delta F_j^{\mathrm{EB.in}}$, $\Delta F_j^{\mathrm{EC.in}}$	incremental electricity consumption costs for EB and EC

$\Delta P_j^{\mathrm{EB.in}}$, $\Delta P_j^{\mathrm{EC.in}}$	incremental electricity consumption powers of EB and EC	$\Delta P_j^{\mathrm{GT.e}}$	incremental electricity generation power of GT
$\Delta P_j^{\mathrm{AC.in}}$	increment in the heat consumption of AC	$\Delta P_j^{\mathrm{GT.h}}$	increment in the heat output of GT
$\Delta P_j^{\mathrm{load.c}}$	increment in the cooling load power	$\Delta P_j^{\mathrm{load.h}}$	increment in the thermal load power
ΔF_j^{DG}	incremental operating cost of DG	$\Delta F_j^{\mathrm{grid}}$	incremental cost of purchasing electricity from the grid
$\Delta P_j^{\mathrm{pur}}$, $\Delta P_j^{\mathrm{sell}}$	increments in power purchase and sale	ΔF_j^{FC}	incremental cost of fuel cells
P_j^{wind}, P_j^{pv}	output of DG from the day-ahead scheduling plan	$\Delta X_j^{\mathrm{pur}}$, $\Delta X_j^{\mathrm{sell}}$	transaction states for power purchase and sale
$\widetilde{P}_{\mathrm{max},j}^{\mathrm{wind}}$, $\widetilde{P}_{\mathrm{max},j}^{\mathrm{pv}}$	intra-day scheduling forecast values DG	$\Delta P_j^{\mathrm{wind}}$, ΔP_j^{pv}	output increments for wind turbines and photovoltaic units
ΔP_j^{FC}	FC output increment	P_j^{FC}	FC's scheduled output from the day-ahead plan
ΔX_j^{FC}	operational state of the fuel cell		

References

1. Xu, Z.; Han, G.; Liu, L.; Martínez-García, M.; Wang, Z. Multi-Energy Scheduling of an Industrial Integrated Energy System by Reinforcement Learning-Based Differential Evolution. *IEEE Trans. Green Commun. Netw.* **2021**, *5*, 1077–1090. [CrossRef]
2. Wang, Y.; Hu, J.; Liu, N. Energy Management in Integrated Energy System Using Energy–Carbon Integrated Pricing Method. *IEEE Trans. Sustain. Energy* **2023**, *14*, 1992–2005. [CrossRef]
3. Cui, Z.; Hu, W.; Zhang, G.; Huang, Q.; Chen, Z.; Blaabjerg, F. A Novel Data-Driven Online Model Estimation Method for Renewable Energy Integrated Power Systems with Random Time Delay. *IEEE Trans. Power Syst.* **2023**, *38*, 5930–5933. [CrossRef]
4. Zheng, L.; Wang, J.; Chen, J.; Ye, C.; Gong, Y. Two-Stage Co-Optimization of a Park-Level Integrated Energy System Considering Grid Interaction. *IEEE Access* **2023**, *11*, 66400–66414. [CrossRef]
5. Li, C.; Yang, H.; Shahidehpour, M.; Xu, Z.; Zhou, B.; Cao, Y.; Zeng, L. Optimal Planning of Islanded Integrated Energy System With Solar-Biogas Energy Supply. *IEEE Trans. Sustain. Energy* **2020**, *11*, 2437–2448. [CrossRef]
6. Daneshvar, M.; Mohammadi-ivatloo, B.; Zare, K.; Anvari-Moghaddam, A. Risk-Aware Stochastic Scheduling of Hybrid Integrated Energy Systems with 100% Renewables. *IEEE Trans. Eng. Manag.* **2024**, *71*, 9314–9324. [CrossRef]
7. Zhang, R.; Chen, Y.; Li, Z.; Jiang, T.; Li, X. Two-Stage Robust Operation of Electricity-Gas-Heat Integrated Multi-Energy Microgrids Considering Heterogeneous Uncertainties. *Appl. Energy* **2024**, *371*, 123690. [CrossRef]
8. Xia, W.; Ren, Z.; Qin, H.; Dong, Z. A Coordinated Operation Method for Networked Hydrogen-Power-Transportation System. *Energy* **2024**, *296*, 131026. [CrossRef]
9. Li, Z.; Xu, Y.; Wang, P.; Xiao, G. Restoration of a Multi-Energy Distribution System With Joint District Network Reconfiguration via Distributed Stochastic Programming. *IEEE Trans. Smart Grid* **2024**, *15*, 2667–2680. [CrossRef]
10. Dong, W.; Lu, Z.; He, L.; Zhang, J.; Ma, T.; Cao, X. Optimal Expansion Planning Model for Integrated Energy System Considering Integrated Demand Response and Bidirectional Energy Exchange. *CSEE J. Power Energy Syst.* **2023**, *9*, 1449–1459.
11. Sheng, T.; Guo, Q.; Sun, H.; Pan, Z.; Zhang, J. Two-Stage State Estimation Approach for Combined Heat and Electric Networks Considering the Dynamic Property of Pipelines. *Energy Procedia* **2017**, *142*, 3014–3019. [CrossRef]
12. Brahman, F.; Honarmand, M.; Jadid, S. Optimal Electrical and Thermal Energy Management of a Residential Energy Hub, Integrating Demand Response and Energy Storage System. *Energy Build.* **2015**, *90*, 65–75. [CrossRef]
13. Shi, M.; Wang, H.; Xie, P.; Lyu, C.; Jian, L.; Jia, Y. Distributed Energy Scheduling for Integrated Energy System Clusters with Peer-to-Peer Energy Transaction. *IEEE Trans. Smart Grid* **2023**, *14*, 142–156. [CrossRef]
14. Yan, M.; He, Y.; Shahidehpour, M.; Ai, X.; Li, Z.; Wen, J. Coordinated Regional-District Operation of Integrated Energy Systems for Resilience Enhancement in Natural Disasters. *IEEE Trans. Smart Grid* **2019**, *10*, 4881–4892. [CrossRef]
15. Huang, J.; Li, Z.; Wu, Q.H. Coordinated Dispatch of Electric Power and District Heating Networks: A Decentralized Solution Using Optimality Condition Decomposition. *Appl. Energy* **2017**, *206*, 1508–1522. [CrossRef]
16. Wang, S.; Wang, S.; Chen, H.; Gu, Q. Multi-Energy Load Forecasting for Regional Integrated Energy Systems Considering Temporal Dynamic and Coupling Characteristics. *Energy* **2020**, *195*, 116964. [CrossRef]
17. Bao, Z.; Zhou, Q.; Yang, Z.; Yang, Q.; Xu, L.; Wu, T. A Multi Time-Scale and Multi Energy-Type Coordinated Microgrid Scheduling Solution—Part I: Model and Methodology. *IEEE Trans. Power Syst.* **2015**, *30*, 2257–2266. [CrossRef]
18. Bao, Z.; Zhou, Q.; Yang, Z.; Yang, Q.; Xu, L.; Wu, T. A Multi Time-Scale and Multi Energy-Type Coordinated Microgrid Scheduling Solution—Part II: Optimization Algorithm and Case Studies. *IEEE Trans. Power Syst.* **2015**, *30*, 2267–2277. [CrossRef]

19. Al-Humaid, Y.M.; Khan, K.A.; Abdulgalil, M.A.; Khalid, M. Two-Stage Stochastic Optimization of Sodium-Sulfur Energy Storage Technology in Hybrid Renewable Power Systems. *IEEE Access* **2021**, *9*, 162962–162972. [CrossRef]
20. Zhou, Z.; Zhang, J.; Liu, P.; Li, Z.; Georgiadis, M.C.; Pistikopoulos, E.N. A Two-Stage Stochastic Programming Model for the Optimal Design of Distributed Energy Systems. *Appl. Energy* **2013**, *103*, 135–144. [CrossRef]
21. Zhang, T.; Li, Z.; Wu, Q.H.; Zhou, X. Decentralized State Estimation of Combined Heat and Power Systems Using the Asynchronous Alternating Direction Method of Multipliers. *Appl. Energy* **2019**, *248*, 600–613. [CrossRef]
22. Yang, H.; Li, M.; Jiang, Z.; Zhang, P. Multi-Time Scale Optimal Scheduling of Regional Integrated Energy Systems Considering Integrated Demand Response. *IEEE Access* **2020**, *8*, 5080–5090. [CrossRef]